Anisotropy of Mechanical Properties of an AZ31 Alloy Prepared by SPD Method

Zuzanka Trojanová [1], Zdeněk Drozd[1,*], Kristián Mathis[1], Michal Kövér [2], Ján Džugan [2], Pavel Lukáč [1] and Kristýna Halmešová [2]

[1]*Charles University, Faculty of Mathematics and Physics, Ke Karlovu 3, CZ-121 16 Praha 2, Czech Republic*
[2]*Comtes FHT, Průmyslová 995, CZ-334 41 Dobřany, Czech Republic*

*Corresponding author: E-mail: zdenek.drozd@mff.cuni.cz; Tel: (+420) 95155 2410

Received: 29 April 2019, Revised: 11 July 2019 and Accepted: 12 July 2019

DOI: 10.5185/amlett.2019.0037
www.vbripress.com/aml

Abstract

Cast magnesium alloy AZ31 was processed by equal channel angular pressing (ECAP); 1-8 passes were applied using different processing routes A, B_C and C. Samples were cut from the extruded billet in the extrusion, transversal and normal directions. Micro-tensile tests were performed at room temperature with an initial strain rate of 1×10^{-3} s^{-1}. The microstructure analysis showed a significant grain reducing. Texture of extruded samples was studied using EBSD technique. The true stress-true strain curves and characteristic stresses exhibit a pronounced anisotropy for all processing routes as a consequence of the developed different texture. Copyright © VBRI Press.

Keywords: Magnesium alloy AZ31, ECAP, tensile tests, anisotropy.

Introduction

Mg-Al-Zn-(Mn) alloys are frequently used magnesium alloys. The alloys strength increases with increasing Al content while ductility decreases. Mg-3Al-1Zn (AZ31) alloy with the low Al content is a typical wrought alloy. Poor plasticity of metals exhibiting low symmetry is done by the shortage of slip systems which are crystallographic equivalent. Owing to the von Mises criterion, slip in both basal and non-basal slip systems are necessary for compatible deformation of AZ31 polycrystals [**1**]. An additional mode of deformation may substitute the slip in a non-basal slip system. While slip of <a> dislocations in basal plane is the soft deformation mode, <a> and <c+a> dislocations operating in non-basal planes represent the hard deformation mode. Another deformation mode, often observed in magnesium and its alloys, is mechanical twinning. Particularly, primary twins $\{10\bar{1}2\}\langle10\bar{1}1\rangle$ may be formed in tension and during the compressive straining [**2**]. Similarly, contraction twins $\{10\bar{1}1\}\{10\bar{1}2\}$ may result in the contraction of the crystal along <c> axis of the hexagonal cell [**3**]. Because of soft and hard slip modes, certain texture is formed during plastic deformation, which is the reason for the observed material plastic anisotropy. This anisotropy may be determined as the tension-compression asymmetry [**4-7**], planar plastic anisotropy of sheets [**8-10**] or anisotropy of dynamic and fracture behaviour [**11, 12**]. Anisotropy of the hexagonal magnesium cell may be also manifested in physical properties as internal friction [**13**], thermal expansion [**14-16**] or thermal conductivity [**17**]. One possibility how to improve mechanical properties of metallic materials is reduction of their grain size via severe plastic deformation (SPD). Different techniques of the SPD were developed in order to obtain bulk material with as low as possible small grain size [**18**]. Among them, equal channel angular pressing (ECAP) is most worldwide used SPD process. There are basically four processing routes in ECAP technique: route A where the sample is extruded without any rotation, route B_A where the sample is rotated in alternate direction between consecutive passes, in B_C route the specimen is rotated by 90° counter clockwise between individual passes and in route C the sample is rotated by 180° between passes [**19**]. The microstructure and texture of samples prepared by various processing routes are different [**20**]. The grain size of ingots produced by the ECAP may be also controlled by processing temperature and the channel geometry. The lower processing temperature the lower grain size [**21-24**]. On the other hand, texture formed during the ECAP is influenced by the processing route: A, B or C. The developed texture is a crucial factor for the strain mechanism operating in tension and compression tests. The effect of the initial texture on plastic anisotropy of rolled AZ31 alloy deformed in compression was studied by Lee and co-workers [**25**]. They estimated distinguish plastic anisotropy in both samples oriented in the rolling direction and in the normal direction, respectively. The effect of processing routes on

mechanical properties of AZ31 alloy submitted to two passes of each route has been presented in [**26**]. Muralidhar *et al.* estimated different microstructures formed in samples processed by different routes; different grain sizes and different deformation behaviours were observed [**26**]. They recommend route B_C as the most favourable to obtain improved mechanical properties. Note, that this result is not generally acceptable. Number of passes and composition of the alloy play also an important role. Krajňák *et al.* [**27**] found a higher strengthening in an AX magnesium alloy ECAPed using route A. Figueiredo *et al.* [**28**] inspected anisotropic behaviour of an ECAPed AZ31 alloy studying the compressive behaviour of the samples at room temperature. An analysis of the strain dependence of the hardening coefficient showed importance of twinning during compressive straining of samples oriented with the stress axis in the extrusion direction. In spite of many papers dealing with ECAPed magnesium alloys, there is no complex study concerning to the microstructure and deformation behaviour of these alloys with respect to the processing routes and samples orientations. We used miniaturised tensile tests for studying plastic anisotropy of samples prepared with various ECAP routes and different number of processing passes. We focused our attention to the tensile properties and deformation mechanisms of ECAPed samples prepared with various processing routes.

Experimental

Gravity cast AZ31 alloy (nominal composition 3 wt.% Al, 1 wt.% Zn, 0.2 wt.% Mn, balance Mg) was annealed at 390 °C for 22 h. The microstructure of the annealed alloy is shown in **Fig. 1**. Billets with dimensions of 10 ×10 ×100 mm^3 were equal channel angular pressed in a rectangular channel 10 × 10 mm^2 (inner angle $\phi = 90°$ outer curvature $\psi = 0°$) at 250 °C and the machine speed of 10 mm/min. Material was subjected to 1, 2, 4 and 8 passes through the ECAP tool using A, B_C and C routes. Samples for micro-tensile deformation were cut from the ECAPed billets so that the loading axis was parallel (ED), transversal (TD) and normal (ND) to the extrusion direction, respectively. The samples microstructure after ECAP was analyzed on three planes: perpendicular to the extrusion direction (X plane), perpendicular to the transversal direction (Y plane) and perpendicular to the normal direction (Z plane) using a light microscope Olympus. For the sample's preparation, the conventional mechanical polishing and etching were carried out using Glycol solution (1 ml HNO_3, 24 ml water, 75 ml ethylene glycol). Texture of samples was estimated by a FEI Quanta 200 FX scanning electron microscope (SEM) equipped with EDAX EBSD system. Microhardness was measured with the Vickers pyramid at room temperature using a Qness 10a apparatus with the load of 0.1 kg. The dwell time was 10 s.

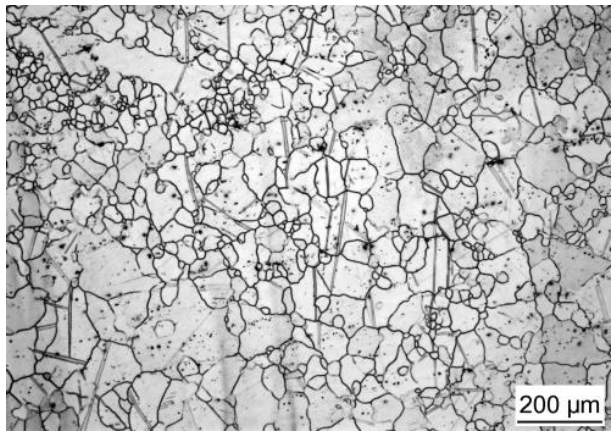

Fig. 1. Microstructure of the cast alloy after thermal treatment.

Because the ECAP technique is usually applied in academic laboratories on relatively small ingots, the miniature tensile test method was developed which allows machining of several specimens oriented into three directions from a billet obtained by the ECAP processing. Tensile experiments were performed on miniaturized samples with the dog bone shape, exhibiting the active gauge length of 3 mm, a width of 1.5 mm and a thickness of 0.5 mm.

The tensile tests were performed at room temperature with an initial strain rate of 10^{-3} s^{-1} in a servo-electric test machine with 5kN load capacity. The strain was measured by the Digital Image Correlation (DIC) technique, implemented in the Aramis software. Naturally, this method may be applied for micro- or nano-grained samples where large number of grains per sample cross-section ensures good reproducibility of experimental results. Authors, who developed this experimental technique, have shown that results obtained for ECAPed AZ31 alloy in miniaturized tensile tests are comparable with those achieved in conventional tests [**29, 30**]. The tensile yield strength (TYS) and ultimate tensile strength (UTS) were estimated from the true stress-true strain curves.

Results and discussion

Light micrographs obtained for samples after the first pass and four passes, prepared by various processing routes are shown in **Fig. 2**. Micro-photos were taken from three planes: perpendicular to the extrusion direction (X plane), perpendicular to the transversal direction (Y plane) and perpendicular to the normal direction (Z plane). Comparing with the original microstructure, it is obvious that a substantial grain refinement was achieved in the first pass through the ECAP device. The microstructure is heterogeneous; smaller grains surround bigger ones.

Grain refinement continued in next passes as shown in **Fig. 2**. It should be mentioned that many grains were significantly refined, some bigger grains can be observed after four passes through the ECAP tool. This is a consequence of dynamic recrystallization which started the microstructure decomposition [**31**].

Copyright © VBRI Press

The most uniform grain structure seems to be in the Z plane. Hilšer and co-workers studying microstructure of magnesium alloy AZ61, subjected to the twist ECA extrusion, found that after three passes original grains were fully replaced with recrystallized grains [**32**]. The grain size, *d*, estimated on the X plane was nearly the same for all processing routes: d_A = 3.57 μm, d_B = 3.43 μm and d_C = 3.97 μm. Slightly higher grain sizes were estimated on Y and Z cross-sections: 3.37-4.81 μm, depending on the processing route. Such values of the grain size 3-4 μm are usually achieved after ECAP at a temperature of 250 °C [**33**]. The grain refinement is saturated after four passes. The grain structure was found most uniform in all planes in the sample prepared using route C. Severe plastic deformation may increase the dislocation density in samples. The evolution of the dislocation density after the ECAP processing was found to be similar in various magnesium alloys [**34-36**]. After a rapid increase in the first pass, the dislocation density continuously decreases down with increasing number of passes, often to the value estimated in the original material. Newly created dislocations contribute to the grain refinement due to sub grains formation and their conversion in a recrystallization process into grains with the high angle grain boundaries (HAGBs). Mathis *et al.* [**37**] estimated the fraction of HAGBs in AZ31 alloy samples processed by four times ECAP at the same conditions as in this study. They found marginal differences between samples prepared with various processing routes; fraction of HAGBs exhibited 85.5 - 92.1 %. The highest fraction of HAGBs was found on all three cross-sections of samples processed with B_C route. The high fraction of the HAGBs indicates good thermal stability of ECAPed samples. Combination of slip deformation in basal and non-basal slip systems and rotation of the crystal lattice during the ECAP processing are the reasons for different texture developed in samples prepared with various processing routes [**27, 37**].

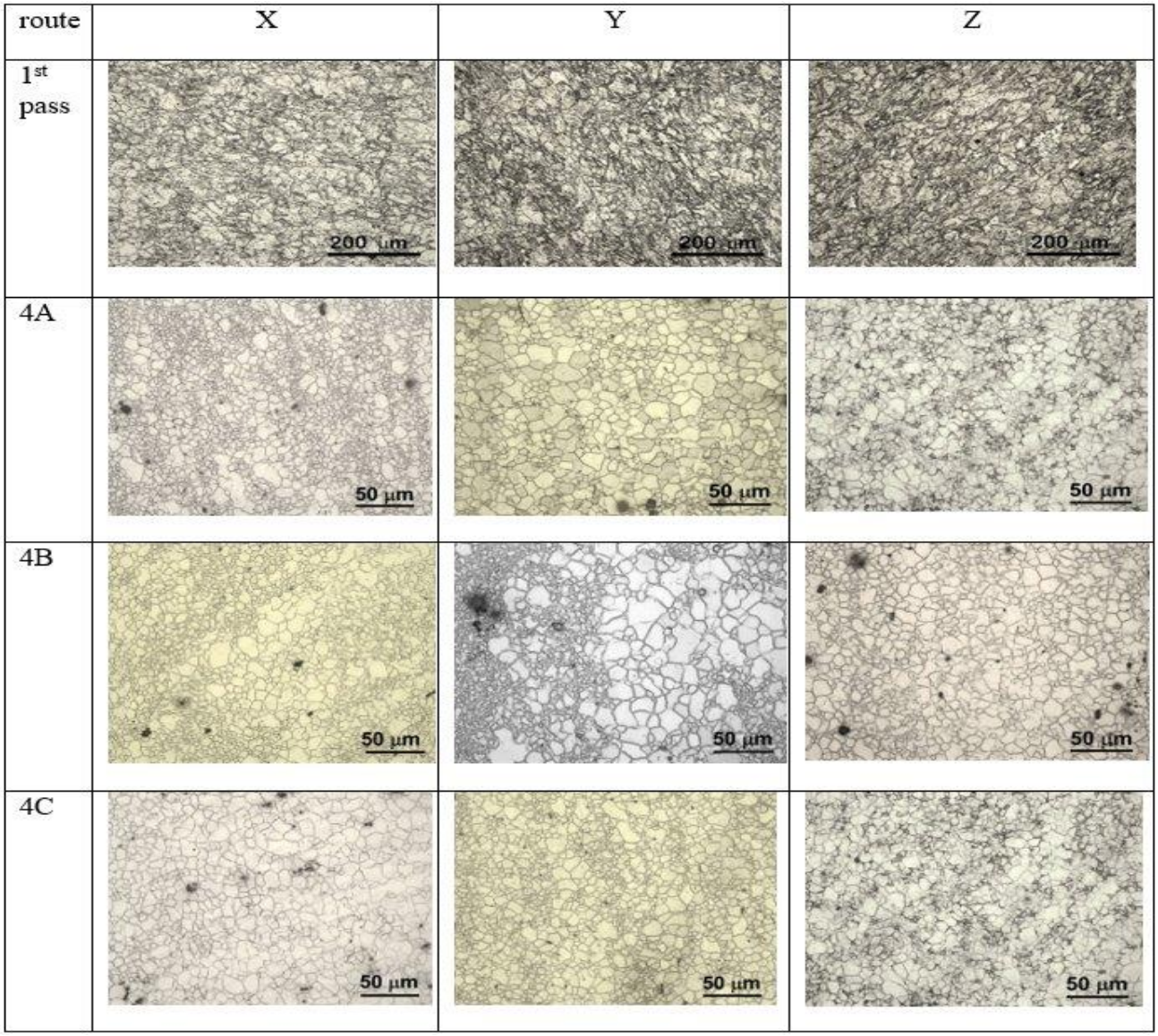

Fig. 2. Microstructure of samples studied after the single pass and four passes through the ECAP device.

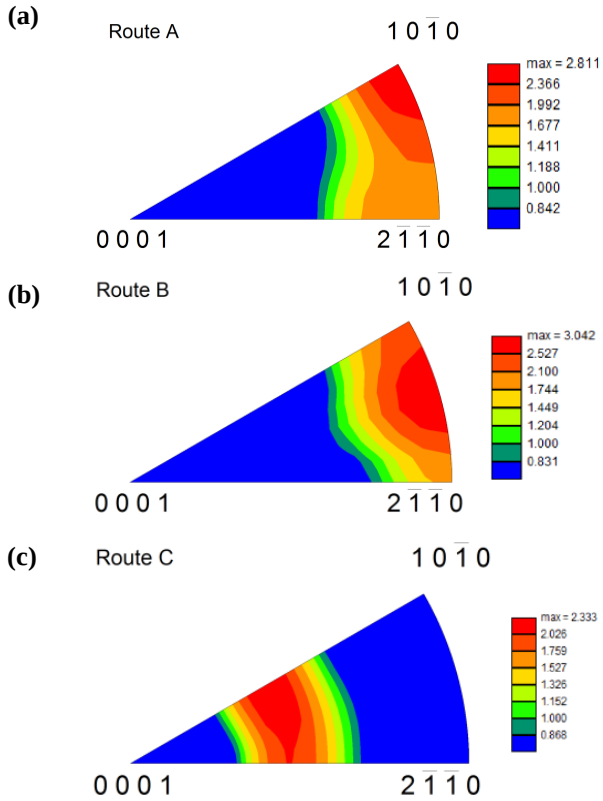

Fig. 3. Inverse pole figures of samples prepared with various processing routes.

The inverse pole figures of samples taken from the X plane are shown in **Fig. 3** for all processing routes. According to our experiences, the texture development is mostly realized in the second pass; texture changes after next passes have been found to be only insignificant.

Microhardness measured on X-planes of four times extruded samples prepared by various processing routes are shown in **Fig. 4**. The estimated values: HV_A = 60.86±4.52; HV_B = 61.30±4.07; HV_C = 57.79±3.35 correspond well with the results of tensile tests; the highest values of the characteristic stresses were found for samples prepared with the B_C route (see **Table 1**). Note that values reported in **Table 1** were estimated in tensile tests while the microhardness test is in principle modified compression creep experiment. Because of known tension-compression asymmetry results; the yield stresses and microhardness values are not simply comparable. Microhardness is nearly uniform in the plane 10x10 mm^2 for all processing routes.

Table 1. Tensile yield stresses (TYS) estimated for various processing routes and number of passes (NP).

Route/TYS (NP) in MPa		TYS(1)	TYS(4)	TYS(8)
A	ED	149	144	124
	TD	211	201	230
	ND	115	117	114
B	ED	149	154	
	TD	211	160	164
	ND	115	131	121
C	ED	149	149	148
	TD	211	231	242
	ND	115	103	96

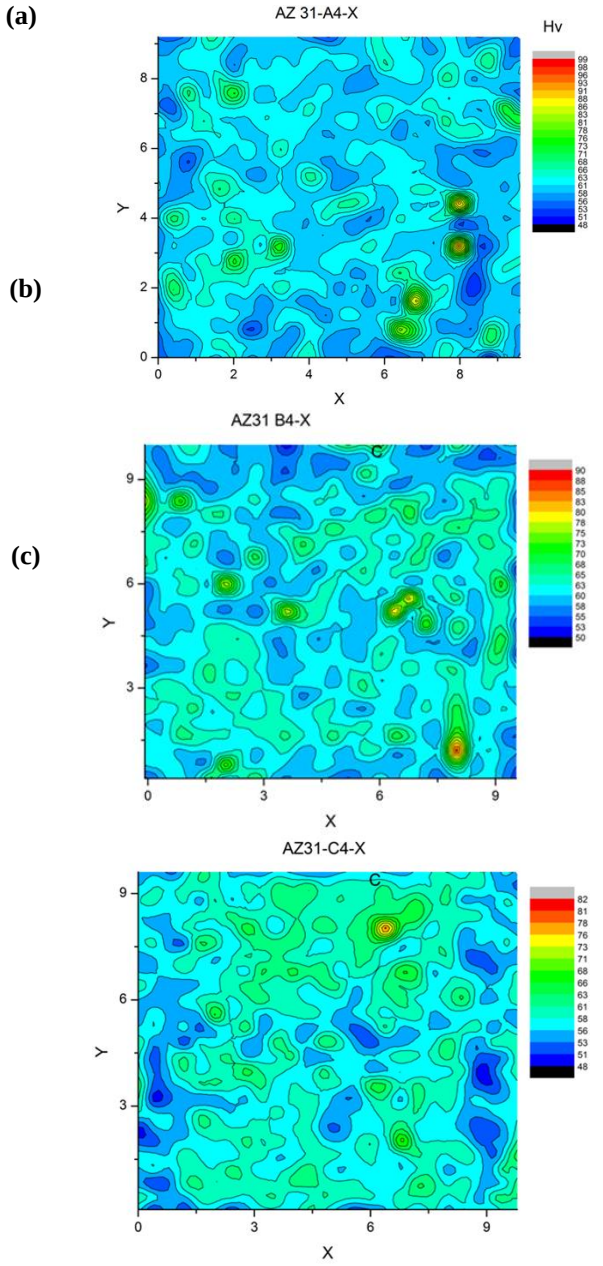

Fig. 4. Microhardness estimated on sections perpendicular to ED (X) and various routes.

The true stress, σ, vs true strain, ε, curves are shown in **Fig. 5** for samples prepared with three processing routes A, B_C and C tested in ED, TD and ND. Inspection of these plot shows that there are differences in the yield strength, ultimate tensile strength and overall shapes of curves reflecting the strain hardening. These differences are due to the different processing history and different tensile axis orientation with respect to the extrusion direction.

The sequence of the curves obtained for various tensile orientations is similar for all the processing routes and number of passes. In the region of lower strains (up to 4-5 %), the highest stresses were achieved for samples oriented in the TD. Slightly lower stresses were found for the ED, the lowest stresses were found for samples oriented in the ND. The highest values of

Copyright © VBRI Press

the strain hardening and strains to fracture exhibit stress-strain curves of samples oriented in the TD. The values of TYS and UTS estimated from true stress-true strain curves for particular directions and processing routes are reported in **Table 1** and **Table 2**.

Comparing estimated values of the TYS with the value found for cast alloy, (TYS(0) = 57 MPa), we may conclude that the strengthening effect of the ECA extrusion is very high already after the single pass; after further passes, the stresses increased less or even decreased. This result is valid for all orientations of the tensile axis with respect to the ED. Similar effects of the sample orientation were found for the UTS values as it follows from **Table 2**.

Table 2. Ultimate tensile strength (UTS) estimated for various processing routes and number of passes (NP).

Route/UTS (NP) in MPa		UTS(1)	UTS(4)	UTS(8)
A	ED	252	253	231
	TD	273	275	291
	ND	269	264	270
B	ED	252	271	
	TD	273	261	266
	ND	269	242	223
C	ED	252	236	249
	TD	273	258	292
	ND	269	216	216

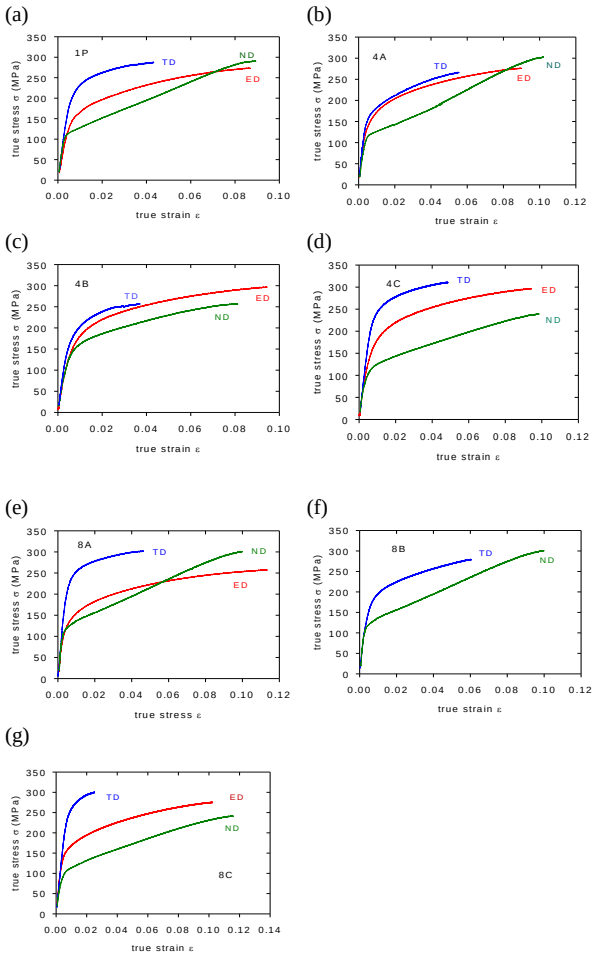

Fig. 5. True stress-true strain curves estimated for samples processed with various routes and number of passes. Anisotropy of ECAPed samples is obvious.

The main strengthening effect was achieved in the single extrusion pass; next passes increased the TYS only slightly or caused a decrease exhibiting until tens MPa. The estimated improvement of the mechanical properties after the single pass may be influenced by i) an increase of the dislocation density and ii) refinement of the grain size. As it was mentioned above, the highest density of new dislocations is generated in the first pass [**34-36**].

Hellmig and co-workers [**38**] measured acoustic emission (AE) signal during compressive straining of single and four times ECAPed AZ31 alloy. They estimated a strong AE signal in the sample after the first pass, which was explained as a collective motion of bigger dislocations ensembles in inhomogeneous microstructure containing coarse residual grains. On the other hand, AE signal was very weak after four passes, if any. It indicates that the dislocation motion, which is considered as the main source of AE, was in the ultrafine grains considerably restricted. TEM revealed no deformation twins in the highly inhomogeneous microstructure [**38**]. Note, that in this case samples were prepared using processing route B_C and they were deformed in the ED. The main strengthening term in the several times ECAPed samples is the Hall-Petch strengthening [**39**]. In our previous paper [**37**], we analysed EBSD measurements of four times processed AZ31 samples prepared with routes A, B_C and C. Schmid factors (SF) were estimated for particular deformation mechanisms: basal slip of <a> dislocations, prismatic slip of <a> dislocations, 2nd order pyramidal slip of <c+a> dislocations and mechanical twinning.

Observed anisotropy of ECAPed samples may be explained by probability of particular slip system (twinning) activity following from the SF value for individual deformation modes. Diverse textures developed in samples using various processing routes are reason for the different SFs estimated in planes perpendicular to ED, TD and ND. Deformation texture developed after ECA extrusion via A and B_C route exhibits a splitting of (0001) poles towards a position rotated of certain angel in a counter-clockwise sense from the normal direction. Prismatic planes $\{10\bar{1}1\}$ and $\{10\bar{1}2\}$ tend to be aligned nearly parallel to the ED. Such orientation of hexagonal cells is favourable for motion of <a> dislocations in basal and prismatic planes. Low SFs found for <a> dislocations are reason for the highest values of the TYS of sample oriented into TD. Slip of <c+a> dislocations in pyramidal planes and twinning are the main deformation modes. The texture developed in the C processing route, with the c-axis nearly oriented into ED, is favourable for twinning. Because the critical resolved stress for twinning is lower than the critical resolved shear stress for dislocation motion, lower values of the TYS are found in C samples in the ND. Twin boundaries are impenetrable obstacles for dislocation motion. This is reason for high work hardening rate observed in ND for all processing routes. Generally, it is possible to

Copyright © VBRI Press

conclude that the strengthening effect of the ECAP and also the TYS increase are saturated in the 4th pass and changes estimated after the 8th pass were found to be marginal. The activity of the twinning decreases with decreasing grain size [**4**]. The main strengthening mode in samples prepared with four and eight passes is the Hall-Petch strengthening. Dislocation motion is restricted with the small grain size and therefore bigger dislocation pile ups are not formed. This was confirmed by the AE measurements in [**38**].

Conclusion

The deformation behavior of ECAPed magnesium alloy AZ31has been examined in tensile tests at room temperature with the aim to find the influence of processing routes and number of passes on the material plastic anisotropy. Main results may be summarized in the following points:

- Pronounced anisotropy of the tensile yield stress and ultimate tensile strength was found for samples prepared with various processing routes and number of passes.
- The highest TYSs were found for samples having the tensile axis in the normal direction of the extruded billets.
- Different texture developed in various processing routs plays important role in controlling of mechanical properties.
- Different deformation mechanisms operating in samples, prepared with various processing routes are responsible for this behavior.
- The main strengthening effect in samples after the single pass is very probably an increase in the dislocation density while the Hall-Petch strengthening plays an important role in several times ECAPed samples.

Acknowledgements

This study was created by project Development of West-Bohemian Centre of Materials and Metallurgy No.: LO1412, financed by the MEYS of the Czech Republic.

Author's contributions

Conceived the plan: ZT, ZD; Performed the expeirments: ZD, MK, KH, KM; Data analysis: ZT, PL, JD, KM; Wrote the paper: ZT. Authors have no competing financial interests.

References

1. von Mises, R.; *Göttin. Nachr. Math. Phys*., **1913**, *4,* 582.
2. Barnett, M. R.; *Mater. Sci. Eng. A*, **2007**, *464,* 1.
3. Barnett, M. R.; *Mater. Sci. Eng. A*, **2007**, *464,* 8.
4. Máthis, K.; Čapek, J.; Zdražilová, Z.; Trojanová, Z.; *Mater. Sci. Eng. A*, **2011**, *528*.
5. Wang, Y. N.; Huang, J. C.; *Acta Mater.*, **2007**, *55,* 897.
6. Trojanová, Z.; Dash, K.; Máthis, K.; Lukáč, P.; Kasakewitsch, A.; *J. Mater. Eng. Perform.*, **2018**, *27,* 3112.
7. Dogan, E.; Karaman, I.; Ayoub, G.; Kiridli, G.; *Mater. Sci. Eng. A*, **2014,** *610,* 220.
8. Trojanová, Z.; Džugan, J.; Halmešová, K.; Németh, G.; Lukáč, P.; Minárik, P.; Bohlen, J.; *Materials*, **2018**, *11,* 73, 1.
9. Balík, J.; Dobroň, P.; Chmelík, F.; Kužel, R.; Drozdenko, D.; Bohlen, J.; Letzig, D.; Lukáč, P.; *Int. J. Plasticity*, **2016**, *76,* 166.
10. Kaiser, F.; Letzig, D.; Bohlen, J.; Styczynski, A.; Hartig, Ch.; Kainer, K. U.; *Mater. Sci. Forum*, **2003**, *315*, 419.
11. Wan, G.; Wu, B. L.; Zhang, Y. D.; Sha, G. Y.; Esling, C.; *Mater. Sci. Eng. A*, **2010**, *527,* 2915.
12. Liu, P.; Xin, Y.; Liu, Q.; *T. Nonferr. Metal. Soc.*, **2011**, *21,* 880.
13. Trojanová, Z.; Drozd, Z.; Lukáč, P.; Minárik, P.; Džugan, J.; Halmešová K.; *Low Temp. Phys.*, **2018**, *44,* 1233.
14. Lukáč, P.; Magnesium Technology: Metallurgy, Design Data, Applications. Friedrich, H.; Mordike, B. L. (Eds.); Springer: Verlag Berlin Heidelberg, **2006**, pp. 63–107.
15. Drozd, Z.; Trojanová, Z.; Halmešová, K.; Džugan, J.; Lukáč, P.; Minárik P.; *Acta Phys. Pol. A*, **2018**, *134,* 820.
16. Trojanová, Z.; Drozd, Z.; Minárik, P.; Lukáč, P.; Kasakewitsch, A., *Thermochim. Acta*, **2016**, *644,* 69.
17. Trojanová, Z.; Halmešová, K.; Drozd, Z.; Šíma, V.; Lukáč, P.; Džugan, J.; Minárik, P.; *Crystals*, 2018, *8,* 278.
18. Estrin, Y.; Vinogradov, A.; *Acta Mater.*, **2013**, 61, 782.
19. Furukawa, M.; Iwahashi, Y.; Horita, Z.; Nemoto, M.; Langdon, T. G.; *Mater. Sci Eng. A*, **1998**, *257,* 328.
20. Agnew, S. R.; Mehrotra, P.; Lillo, T. M.; Stoica, G. M.; Liaw, P. K.; *Acta Mater.*, **2005**, *53,* 3135.
21. Ding, S. X.; Chang, C. P.; Kao, P. W.; *Metal. Mater. Trans. A*, **2009**, *40*, 415.
22. Seipp, S.; Wagner, M.F.-X.; Hockauf, K.; Schneider, I.; Meyer, L. W.; Hockauf, M.; *Int. J. Plasticity*, **2012**, *35,* 155.
23. Bryla, K.; Dutkievicz, J.; Malczewski, P.; *Arch. Mater. Sci. Eng*., **2009**, *40,* 17.
24. Jin, L.; Lin, D.; Mao, D.; Zeng, X.; Chen, B.; Ding, W.; *Mater. Sci. Eng. A*, **2006**, *423,* 247.
25. Lee, B. H.; Park, S. H.; Hong, S-G.; Park, K. T.; Lee, C. S.; *Mater. Sci. Eng. A*, **2011**, *528,* 1162.
26. Muralidhar, A.; Nanendrarath, S.; Shivanda Nayaka, H.; *Proc. Mat. Sci.*, **2014**, *5,* 1560.
27. Krajňák, T.; Minárik, P.; Gubicza, J.; Máthis, K.; R. Kužel, R.; Janeček. M.; *Mater. Charact*., **2017**, *123,* 282.
28. Figueiredo, R. B; Száraz, Z.; Trojanová, Z.; Lukáč, P.; Langdon, T. G.; *Scripta Mater*., **2010**, *63,* 504.
29. Procházka, R.; Džugan, J.; Köver, M.; *Arch. Mater. Sci. Eng.*, **2015**, *76,* 134.
30. Džugan, J.; Konopík, P.; Procházka, R.; Trojanová, Z.; *Mater. Sci Forum*, **2017**, *879,* 471.
31. Sakai, T.; Belyakov, A.; Kaibyshev, R.; Miura, H.; Jonas, J. J.; *Prog. Mater. Sci*., **2014**, *60,* 130.
32. Hilšer, O.; Rusz, S.; Szandera, P.; Čížek, L.; Kraus, M.; Džugan, J.; Maziarz, W.; *Metals*, **2018**, *8,* 776.
33. Gzyl, M.; Rosochowski, A.; Boczkal, S.; Olejnik, L.; *Mater. Sci. Eng. A*, **2015**, *638,* 20.
34. Minárik, P.; Král, R.; Čížek J.; Chmelík, F.; *Acta Mater*., **2016**, *107,* 83.
35. Balogh, L.; Figueiredo, R. B.; Ungár, T.; Langdon, T. G.; *Mater. Sci. Eng. A*, **2010**, *528,* 533.
36. Vrátná, J.; Janeček, M.; Čížek, J.; Lee, D. J.; Yoon, E. Y.; Kim, H. S.; *J. Mater. Sci*., **2013**, *48,* 4705.
37. Máthis, K.; Köver, M.; Stráská, J.; Trojanová, Z.; Džugan, J.; Halmešová, K.; *Materials*, **2018**, *11,* 1644.
38. Hellmig, R. J.; Lamark, T. T.; Popov, M. V.; Janeček, M.; Estrin, Y.; Chmelík, F.; *Mater. Sci. Eng. A*, **2007**, *462,* 111.
39. Yamashita, A.; Horita, Z.; Langdon, T. G.; *Mater. Sci. Eng. A*, **2001**, *300,* 142.

Copyright © VBRI Press